Effect of annealing atmosphere on the luminescence characteristics of CVD−ZnSe

© V.P. Kalinushkin[1], A.A. Gladilin[1], O.V. Uvarov[1], S.A. Mironov[1,¶], V.A. Chapnin[1], M.I. Studenikin[1], N.N. Il'ichev[1], E.M. Gavrishchuk[2], S.A. Rodin[2], N.A. Timofeeva[2]

[1] Prokhorov General Physics Institute of the Russian Academy of Sciences, 119991 Moscow, Russia
[2] Institute of Chemistry of High-Purity Substances named after G.G. Devyatykh of the Russian Academy of Sciences, 603951 Nizhny Novgorod, Russia

¶ E-mail: sa.mironov@kapella.gpi.ru

Received August 20, 2021
Revised August 27, 2021
Accepted August 27, 2021

The influence of the atmosphere of CVD−ZnSe annealing carried out in modes close to the procedure of their doping with iron on the luminescent characteristics of these crystals is investigated. It was found that annealing in the atmosphere of argon and selenium leads to a qualitative change in the impurity-defect composition and to a complex spatial distribution of the luminescent characteristics of CVD−ZnSe, especially in the crystal region at a distance of up to 400 microns from the surface. In the case of annealing in zinc, the luminescent characteristics are more uniform, with the exception of the near-surface zone with a width of about 100 microns, which has a high luminescence intensity in the entire spectral range under study (0.44−0.72 microns). The obtained results are interpreted on the basis of the assumption about the evaporation of zinc during annealing in argon and selenium. Based on the analysis of the spatial distribution of luminescence, assumptions are made about the nature of the observed impurity-defect centers.

Keywords: two-photon confocal microscopy, CVD−ZnSe, impurity-defect composition, high temperature annealing.

DOI: 10.21883/SC.2022.01.53022.9731

1. Introduction

ZnSe doped with Fe and Cr is actively used for creation of IR range lasers [1–3]. The possibility of creation of laser systems, in which an inverse population of Fe and Cr ions is made not with optical pumping, but with impact ionization with hot electrons, is studied [4,5]. These works require detailed study of impurity-defect composition of crystals used for that purpose and influence of various process operations and annealing on it. In many cases the creation of laser crystals is performed using high temperature (900−1250°C) diffusion doping of zinc selenide with Fe and Cr ions. Polycrystal ZnSe, synthesized during chemical vapor deposition (CVD), or CVD−ZnSe [1–3,5–8], is used as a basis. In these cases the annealing of crystals is performed along with diffusion [6–8]. As per the abovementioned, the influence of annealing in various atmospheres (Ar, Se, Zn) in modes, close to doping with Fe, on impurity-defect composition in polycrystal CVD−ZnSe is of interest. In this study the influence of annealing on spatial distribution of luminescence in a range of $0.44-0.72\,\mu$m is examined. Two-photon confocal microscopy (TPCM) will be used as a study method, allowing to examine the spatial distribution of luminescence over the whole volume of crystal with thickness of below 3 mm and with resolution of several micrometers. While there are many studies of annealing influence on ZnSe luminescence [9–12], such experiments are performed for the first time, as far as we know.

2. Experimental scheme

In the study the initial and annealed at temperature of 1000°C polycrystal CVD−ZnSe, produced as a result of zinc and hydrogen selenide vapors reaction in argon flow, was examined. Samples of parallelepiped shape with dimensions of $8 \times 6 \times 4$ mm were cut from the plate part with homogeneous microstructure. Material transmission in spectral range of $2-14\,\mu$m was $\sim 70\%$. For annealing the samples were put into quartz vessels, that were connected to forevacuum pump and argon source. Vessels were washed with argon five times, that allowed to reduce concentration of impurity, caused by the atmosphere (N_2, O_2, CO_2, H_2O). Then Ar was filled to the vessel in such way, that its pressure at set annealing temperature was ~ 1 atm, and then the vessels were sealed. Vessels with constriction were used for making the experiment in matrix components pairs. The examined samples were in one part of the vessel, and Zn or Se sub-samples — in another. The sub-samples mass was selected by means of calculation to provide the matrix component vapor pressure of ~ 1 atm at thermal annealing temperature. CVD−ZnSe samples location was such that all sample surfaces were exposed. Annealing was performed in laboratory thermostat SNOL 6/12 at temperature of 1000°C

for 72 h. Cooling of vessels with samples was performed with turned off thermostat. Then the vessels were opened, samples were removed and subject to mechanical polishing. Luminescence characteristics study was performed using two-photon confocal microscopy. In this study the confocal microscope Carl Zeiss LSM 710 NLO was used. Two-photon excitation was performed with variable wavelength laser in a range of $0.71-1.05\,\mu$m (radiation with wavelength of $0.8\,\mu$m was used in this study). Pulse duration was 150 fs, frequency was 80 MHz, maximum average power of $0.1-1$ W varied depending on detection conditions and was optimized for receiving the contrast image of the sample luminescence. Luminescence spectra was registered in a range of 440–725 nm with spectral resolution of 10 nm. These parameters fit well for studying the crystal ZnSe, which forbidden band width at room temperature is ~ 2.7 eV. Thus, effective implementation of two-photon excitation and registration of the edge and defect-impurity luminescence are possible on this device (in a range of 460–715 nm). Existing experimental equipment allowed to register and process three-dimensional images of distribution of the edge and defect-impurity luminescence of initial and doped with Fe ZnSe crystals to a depth of up to 3 mm with spatial resolution of several micrometers. Time, required for a single three-dimensional „map" with a depth of 1 mm, with a step of $25\,\mu$m and dimensions of the „flat" map of 1×1 mm was ~ 5 min. All experiments were performed at room temperature. This technique is described in detail in [13,14].

3. Experimental results

The study is focused on influence of CVD–ZnSe annealing on spatial distribution of luminescence characteristics in the abovementioned modes. Figure 1 shows flat maps of initial CVD–ZnSe, made on depth of $100\,\mu$m on luminescence wavelengths of 473 nm (Fig. 1, *a*), 520 and 473 nm (Fig. 1, *b*), and 715 nm (Fig. 1, *c*), and luminescence spectra of various crystal regions. These maps were typical for all samples of initial CVD–ZnSe examined in this study. Luminescence characteristics of these crystals were rather homogeneous on a macroscopic scale. Grain structure of crystals is well observed on the presented maps. Grain sizes were about several dozens of micrometers. Luminescence intensity inside the grains significantly varied. Grain boundaries were usually characterized with low luminescence intensity (Figs. 1, *a* and 1, *b*). However, in individual regions of grain boundaries the bright dots with size of several microns are observed in impurity-defect range of luminescence (Fig. 1, *b*). Figures 1, *a* and 1, *b* show the luminescence spectra of various regions with size of several dozens of micrometers and bright dots. These results were typical for initial CVD–ZnSe. It can be seen, that in the largest part of the crystal the radiation line with wavelength of 463–473 nm (Fig. 1, *a*, curves *1–3*) prevails, that in studies [9,15] were associated with exciton radiation. Impurity-defect centers (IDC) low-intensity luminescence is also registered — a line with intensity maximum near 520 nm with wide long-wave tail of up to 600,nm, and weaker-intensity (on the verge of equipment sensitivity) lines of red luminescence from 650 to 725 nm (see insert in Fig. 1, *a*, curves *1–3*). Luminescence with maximum near 520 nm and long-wave tail of up to 580 nm (hereinafter — line 520) dominates the bright dot. Exciton radiation line is also registered, but it has the weaker intensity than line 520 (Fig. 1, *b*, curves *1–3*). With great probability we can assume that IDC radiation, observed at „integral" measurements, mainly consists of line 520, which blended with weaker radiation of other IDC near 540–600 nm. This part of luminescence spectrum can be the results of several lines summation. Also Fig. 1, *c* shows that the red luminescence is distributed along the crystal rather homogeneously and looks like luminescence of small dots.

The study is focused on influence of CVD–ZnSe annealing on spatial Figure 2 shows flat maps of CVD–ZnSe (ZnSe–Ar) annealed in argon, made on depth of $100\,\mu$m on luminescence wavelengths of 473 (Fig. 2, *a*), 512 and 715 nm (Fig. 2, *b*), and 570 nm (Fig. 2, *c*). In the selected region on the flat map the dependencies of luminescence intensity on wavelengths of 473, 512, 570 and 715 nm are registered (Fig. 2, *b*). Figure 2, *a* shows luminescence spectra from various sample regions. According to this figures, the sample can be divided into at least two regions — region *1*, adjacent to surface, with width of $\sim 300\,\mu$m, where exciton luminescence and IDC in a range below 520 nm are minimized, and region *2* inside the sample. Region *1* appears as wide strip, parallel to surface. It consists of two sub-bands. In the first one, with a width of $200\,\mu$m, adjacent to surface, the spectrum consists of low-intensity exciton luminescence line and IDC luminescence in a range from 520 to 620 nm with maximum near 560 nm (strip 560), as well as red lines luminescence (Fig. 2, *a, c*, curve *1*, see insert, curve *1*). Another sub-band, located behind the first one, is characterized with low intensity of IDC luminescence in a range from 480 to 650 nm. It has the relatively low exciton and red luminescence (Fig. 2, *a, c*, curve *2*, see insert, curve *2*). This sub-band also appears as a strip with a width of $\sim 100\,\mu$m, parallel to sample surface. Boundaries of sub-bands *1.1* and *1.2* become distorted when crossing the grain boundaries (Fig. 2, *b, c*). Considering, that diffusion along the grain boundaries has its own specifics, this fact confirms the assumption that these sub-bands were formed by diffusion processes. In the region *2* the exciton luminescence dominates the spectrum and IDC luminescence strip with intensity maximum near 520, 540 and 560 nm and long-wave tail of up to 650 nm (strip 520–560) and weak red lines luminescence with maximums near 680 and 715 nm are registered (Fig. 2, *a, b*, curves *3, 4*). Most likely, the strip 520–560 is a result of several lines addition, including strip 560. Part of region *2*, adjacent to region *1*, with a width of $\sim 400\,\mu$m has a bit higher luminescence intensity in the whole spectral

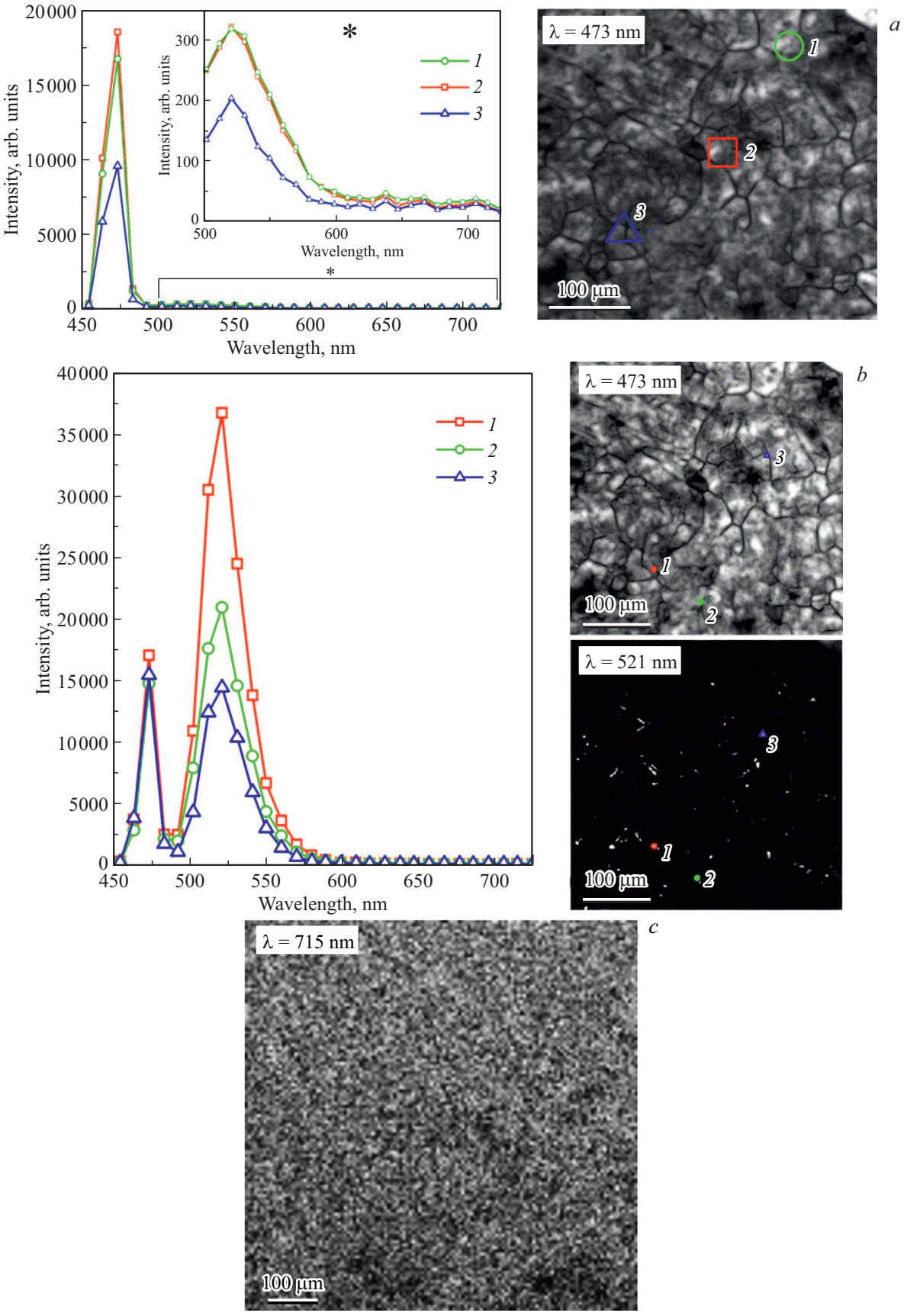

Figure 1. *a* — luminescence map of initial ZnSe on a wavelength of 473 nm and luminescence spectra from the regions selected on the map; *b* — luminescence maps of initial ZnSe on wavelengths of 473 and 520 nm and luminescence spectra of the „bright“ dots selected on the maps; *c* — luminescence map of initial ZnSe on a wavelength of 715 nm.

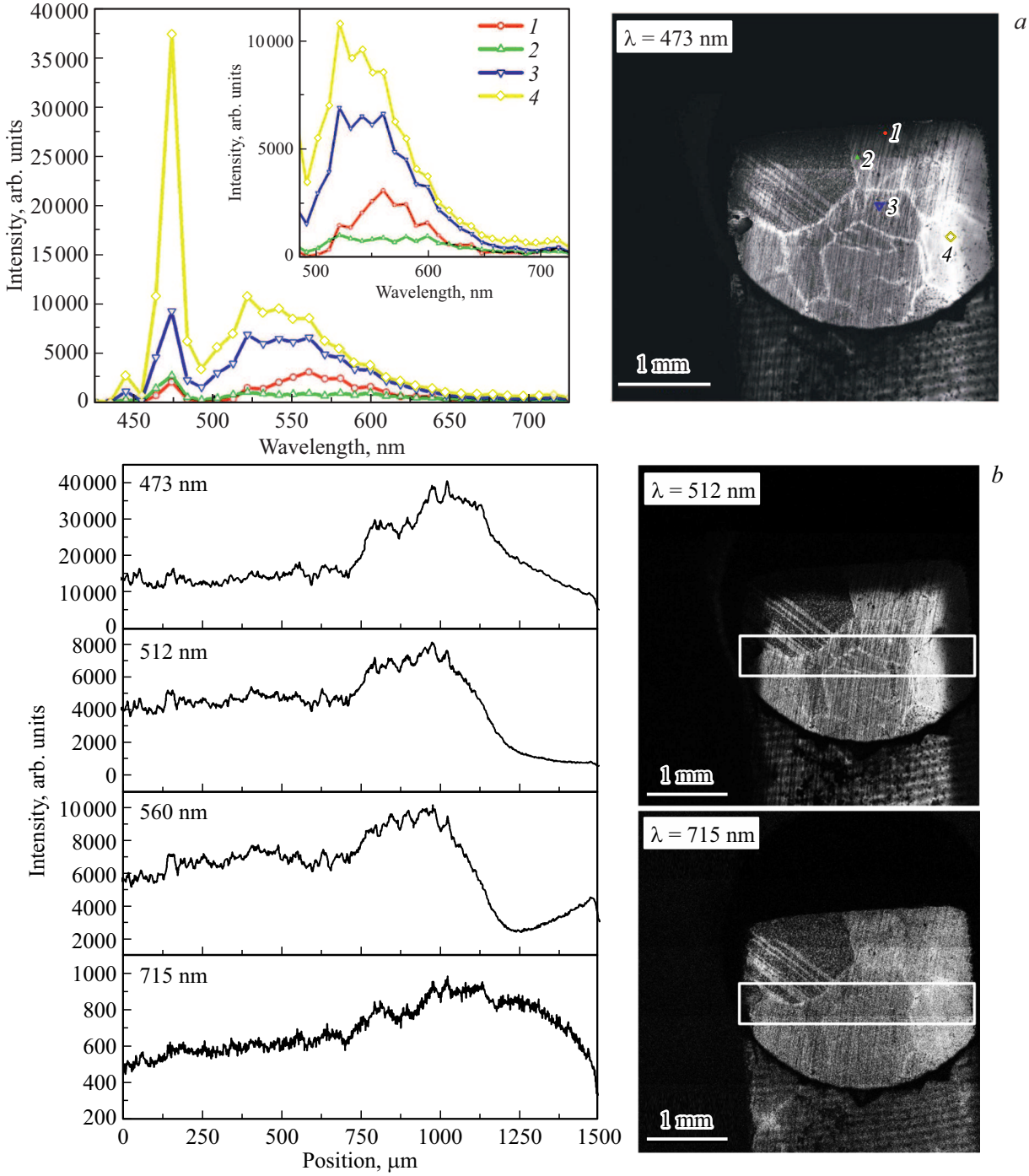

Figure 2. *a* — map of ZnSe–Ar luminescence on wavelength of 473 nm and luminescence spectra from the regions selected on the map: curve *1* — band 1.1, curve *2* — band 1.2, curve *3* — band 2.1, curve *4* — band 2.2; *b* — maps of ZnSe–Ar luminescence on wavelengths of 512 and 715 nm and dependencies of luminescence intensity at the distance from the crystal edge on wavelengths of 473, 512, 560 and 715 nm; *c* — maps of ZnSe–Ar luminescence on wavelengths of 560 nm and luminescence spectra from various crystal bands: curve *1* — band 1.1, curve *2* — band 1.2, curve *3* — band 2.1, curve *4* — band 2.2.

range (sub-band *2.1*), than central band of crystal — sub-band it2.2 (Fig. 2, *a, b*, curves *3, 4*). Grain sizes significantly increased and are $> 500\,\mu$m. In exciton luminescence range the grain boundaries luminesce in a classical way — low luminescence intensity narrow „dark“ core of grain boundary and high luminescence intensity „light“ region around them (Fig. 2, *a*). In spectrum part of 500–560 nm in the region *1* and sub-band *2.1* of crystal the grain boundaries have lower luminescence intensity, in the sub-band *2.2* the grain boundaries luminescence in this range is of similar exciton luminescence type (Fig. 2, *b*). In spectrum part of 570–650 nm the grain boundaries have

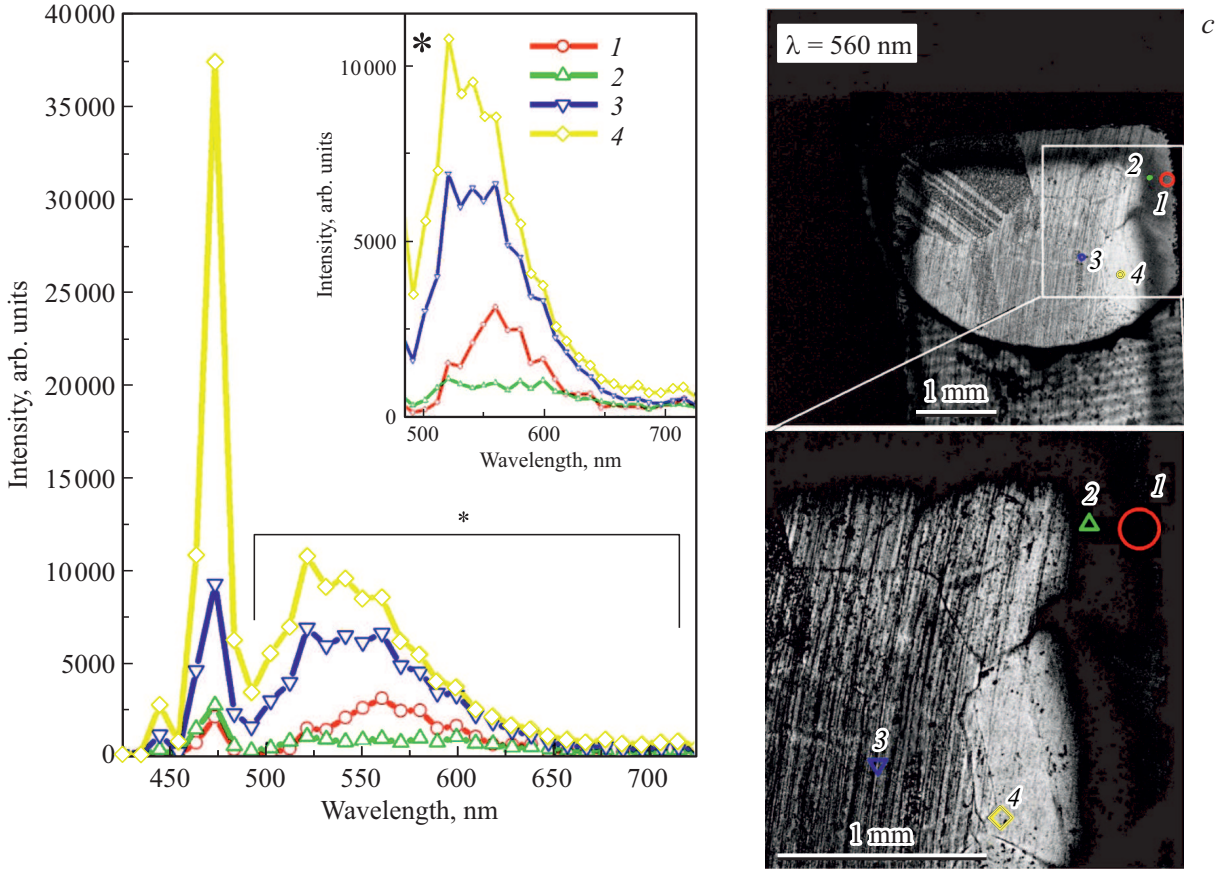

Fig. 2 (*cont.*).

dark contrast, i.e. low luminescence intensity in all regions of crystal (Fig. 2, *b*). In spectral region of 670–715 nm the grain boundaries have higher luminescence intensity in all crystal bands (Fig. 2, *b*). Since samples were mechanically polished, the narrow ($\sim 10\,\mu$m) sub-surface band contains large amount of structure defects. This region luminescence has primarily low intensity in all spectral ranges. As per Fig. 2, *b*, the dependence of exciton luminescence intensity at distance from crystal surface is the following: growth from almost zero at crystal boundary in the band *1* and in the half of the sub-band *2.1*. The luminescence intensity maximum is registered at a distance of $\sim 550\,\mu$m from the sample surface. After that it decreases and reaches plateau at a distance of $\sim 750\,\mu$m from surface. Plateau intensity is comparable with exciton luminescence intensity in the sub-band *1.2*. Luminescence intensity of strip 520–560 in the band *1* is probably close to zero. Then it starts to grow fast, reaching the maximum almost at the same place where exciton luminescence intensity maximum is. With increasing the distance from surface the luminescence intensity of strip 520–560 starts to drop. At distance of $\sim 750\,\mu$m from crystal surface it reaches the plateau (Fig. 2, *b*). Thus, in the region *2* the spatial distribution of the dependence of luminescence intensity in this spectral region is close to similar dependence for exciton. Luminescence intensity of strip 560 has the maximum in the sub-band *1.1*, then it drops in the sub-band *1.2*. In this crystal band it is similar to the increased luminescence intensity region (ILIR) [14,16], adjacent to the sample edge and observed earlier. Then it repeats the spatial distribution of luminescence intensity of strip 520–560 (Fig. 2, *b*). It is possible that spectra of these IDC luminescence overlap partially. Therefore, it is possible that spatial distribution of the dependence of luminescence intensity in the region *2* within a spectral range is defined not by strip 560 nm. The difference of grain boundaries luminescence in the region *2.2* should be noted. Increased luminescence intensity is observed in spectral range of 520–560 nm, reduced — in spectral range of 570–650 nm. The spatial distribution of red lines luminescence intensity is a bit different. The initial fast growth from zero is in the band near surface with a width of $100\,\mu$m. Then, at distance of $\sim 400\,\mu$m from crystal surface the growth slows down with reaching the maximum. Then, the slow decrease is observed with reaching the plateau at distance of ~ 750–$800\,\mu$m from the surface (Fig. 2, *b*). As per fig. 2, *a*–*c* and abovementioned dependencies of luminescence intensity at the distance from the sample surface, the sub-band *1.2* is a strip with a width of $100\,\mu$m, going parallel to crystal surface with reduced

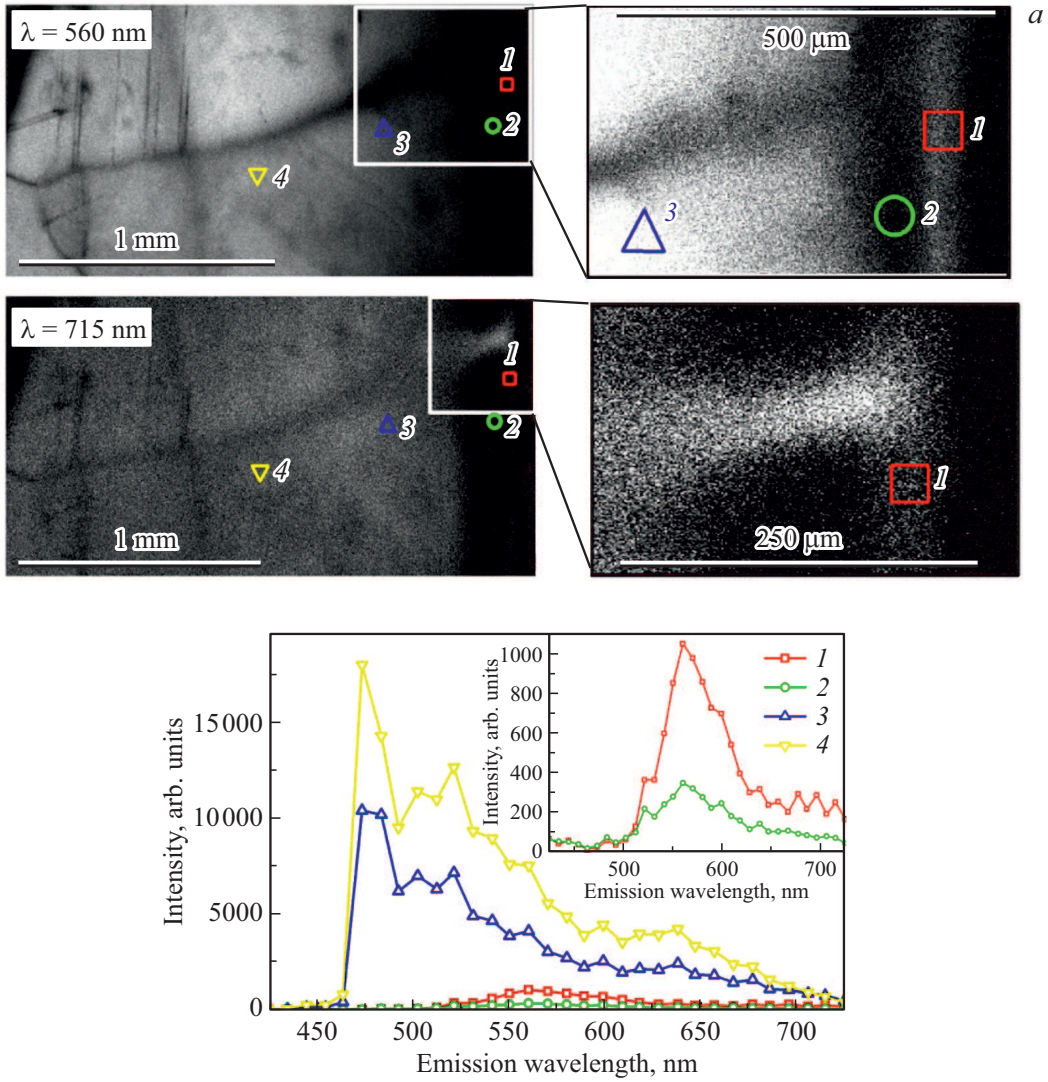

Figure 3. *a* — maps of ZnSe–Se luminescence on wavelengths of 560 and 715 nm and luminescence spectra from various crystal bands: curve *1* — band *1.1*, curve *2* — band *1.2*, curve *3* — band *2.1*, curve *4* — band *2.2*; *b* — maps of ZnSe–Se luminescence on wavelengths of 512 and 473 nm (left part of the figure) and dependencies of luminescence intensity at the distance from the crystal edge on wavelengths of 473, 512, 560 and 715 nm.

impurity luminescence intensity (RLIR) in spectral range of 500–650 nm, similar in shape to ILIR. At the same time it is possible that luminescence in other spectral ranges dominates this crystal region. Figure 3 shows flat maps of CVD–ZnSe (ZnSe–Se) annealed in selenium, made on depth of 100 μm on luminescence wavelengths of 473, 512 (Fig. 3, *c*), 570, 715 nm (Fig. 3, *a*).

The study is focused on influence of CVD–ZnSe annealing on spatial In the region selected on the flat rectangle map the dependencies of luminescence intensity on wavelengths of 473, 512, 570 and 715 nm are observed (Fig. 3, *b*). These results are typical for that sample. Figure 3, *a* shows luminescence spectra from various sample regions. It is shown that as per the luminescence nature, ZnSe–Se sample, as in case of ZnSe–Ar, can be divided into at least two regions — region *1*, adjacent to surface, where exciton and impurity-defect centers (IDC) luminescence in a range below 520 nm are minimized, and region *2* inside the sample. Region *1*, as in case of ZnSe–Ar, is located along the sample edges and appears as a strip, parallel to a surface with a width of 200 μm. Region *2* is characterized with large exciton luminescence and IDC luminescence intensity with maximum near 500, and 520 nm — strip 520–540 and long-wave tail of up to 650 nm, where the maximum is clearly observed near 630 nm (Fig. 3, *a*, curves *3, 4*). Also the exciton line broadening appears clearly, that probably was related to appearance of another line with maximum near 483 nm. As in case of ZnSe–Ar crystals, band *2* can be conditionally divided into two sub-bands. However, unlike ZnSe–Ar in the sub-band *2.1*, adjacent to band *1*, the intensity of the exciton luminescence and

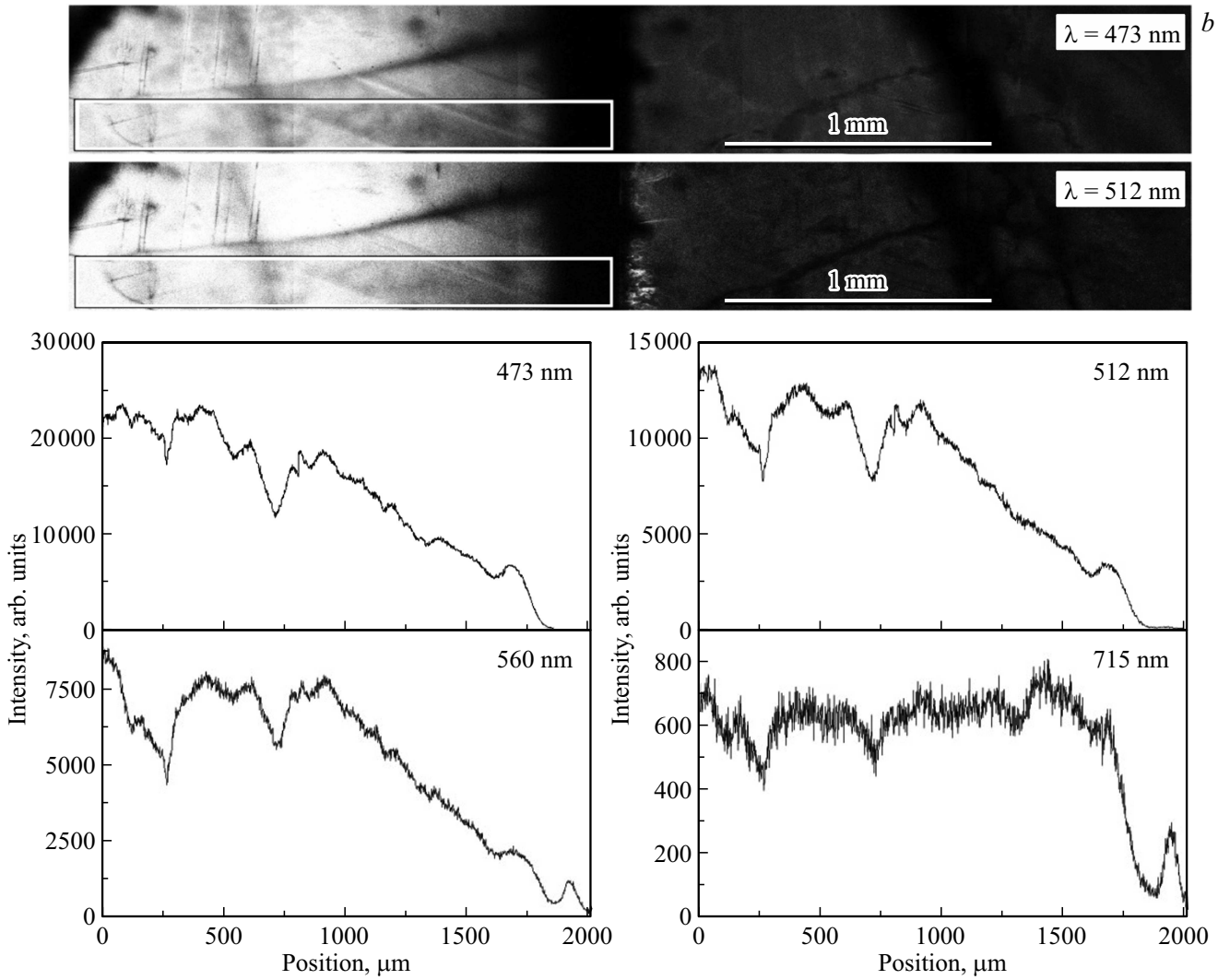

Fig. 3 (*cont.*).

strip 500−520 is a bit less, than in the central band (sub-band *2.2*), while its slow rise is observed in its spectral interval. In crystal center in the band *2.2* the luminescence intensity becomes relatively homogeneous. Band *1*, same as in ZnSe−Ar samples, is divided into two sub-bands. However, unlike ZnSe−Ar samples in the sub-band *1.1* of ZnSe−Se there is almost no exciton luminescence. Luminescence, similar to strip 560 in ZnSe−Ar crystals, and red luminescence dominate it (Fig. 3, *a*, curve *1*, see insert, curve *1*). Width of sub-band *1.1* is $\sim 120\,\mu$m. Band *1.2* is next, where luminescence is minimum in the whole spectral range registered in this study (RLIR). RLIR width is $60-80\,\mu$m (Fig. 3, *a*, curve *2*, see insert, curve *2*). Grains size in ZnSe−Se also increased, but unlike ZnSe−Ar the situation with grain boundary luminescence became complicated. Most likely, grains boundaries, that intersect region *1* of the sample, have low luminescence intensity almost in the whole spectral interval registered in this study. Exception — part of grain boundary in the region *1*, where the intensive red luminescence is observed (Fig. 3, *a, b*). However, it seems that grains boundaries, not contacting with the region *1*, have the luminescence characteristics, regular for grains boundaries: weak luminescence intensity in the middle of the grain boundary and stronger — in the area around it. Near-surface band, same as in ZnSe−Ar, is characterized with low luminescence intensity in the whole spectral range.

Thus, the dependence of luminescence intensity on the distance from crystal surface for exciton is the following. In the band *1*, this is a plateau of very low intensity (probably, there is no exciton luminescence in this part of the crystal). In the end of the band *2.1* — fast rise of luminescence intensity, slowing at depth of $\sim 250\,\mu$m, with reaching the plateau at distance of $\sim 1000\,\mu$m from the crystal surface. The similar dependence for luminescence intensity is in the spectral range of 492−540 nm (Fig. 3, *b*). For luminescence intensity in spectral range of 560 nm the

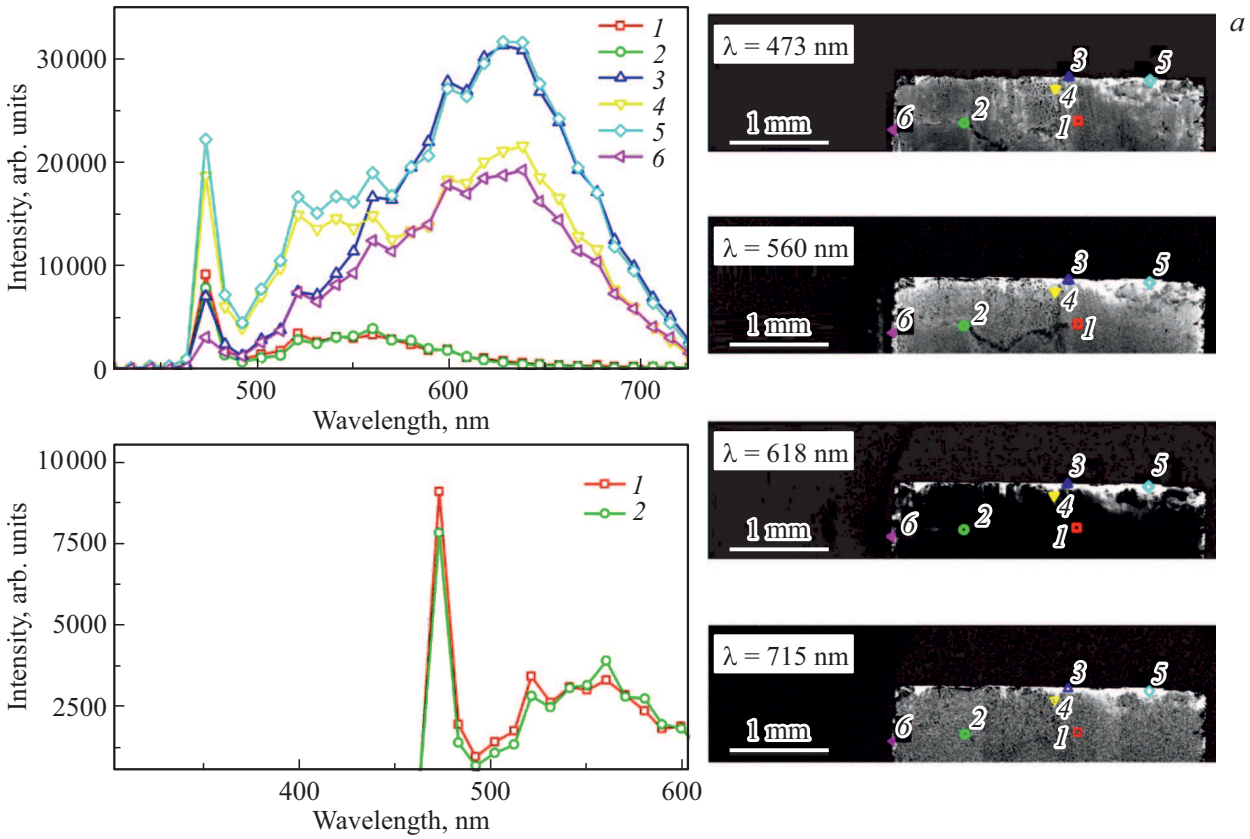

Figure 4. *a* — maps of ZnSe–Zn luminescence on wavelengths of 560 and 715 nm and luminescence spectra from various crystal bands: curves *1, 2* — characterizing crystal volume, curves *3, 5, 6* — characterizing near-surface region, curve *4* — from grain boundary region; *b* — maps of ZnSe–Zn luminescence on wavelength of 473 nm and dependencies of luminescence intensity at the distance from the crystal edge on wavelengths of 473, 512, 560 and 715 nm.

situation is more complicated. In the sub-band *1.1* there is a typical region of ILIR with a width of $\sim 60\,\mu$m. In the remaining volume the spatial distribution of luminescence intensity is close to the similar dependence for excitons and luminescence in a range of 492–540 nm, but with a bit less, than in case of exciton line and strip 500–520 in the band *1.2*, rate of luminescence increase in this spectral range. It is possible that, as in case of ZnSe–Ar, the spatial dependence of luminescence intensity in the region *2* of the crystal is defined not with strip 560, but with long-wave tail of strip 500–520. Dependence of the red luminescence intensity in the band *1* is close to the similar dependence of line 560 — ILIR in the band *1.1*. Then comes the sharp growth of intensity, that at distance of $250\,\mu$m from the surface (in the same place where the bend of the rate increase of exciton and other lines is happened) reaches the plateau. Figure 4 shows the flat maps of luminescence of CVD–ZnSe (ZnSe–Zn), annealed in zinc vapors, made on wavelengths of 473, 540, 618 and 715 nm at distance of $100\,\mu$m from the crystal surface.

In the region selected on the flat rectangle map the dependencies of luminescence intensity on wavelengths of 473, 540, 618 and 715 nm are observed (Fig. 4, *b*). These results are typical for that sample. Figure 4, *a* also shows the spectra from various crystal bands. Unlike ZnSe–Ar and ZnSe–Se crystals, this material has no typical band *1*, the intensive luminescence of exciton and IDC is observed with maximums of 520, 540, 560 nm, similar to IDC luminescence 520–560 in ZnSe–Ar (Fig. 4, *a*, curves *1, 2*). On a macroscopic scale the sample is homogeneous (Fig. 4). However, the band at crystal surface, unlike ZnSe–Ar and ZnSe–Se crystals, is characterized with high exciton and impurity-defect luminescence intensity (Fig. 4, *a*, curves *3, 4, 6*). IDC spectra are wide and often occupy the whole spectral interval. Strips, similar to strip 520–560, and strip with maximum near 630 nm are registered in them (Fig. 4, *a*, curves *3, 4–6*). This band is not similar to ILIR. It is non-homogeneous spatially (Fig. 4, *a*) and appears as decoration of large defects at the surface and, in some cases, spreads to the crystal volume to $50–100\,\mu$m. In cases when grain boundary reaches this band, its luminescence at depth of $200–300\,\mu$m is of type, typical for the surface layer (Fig. 4, *a*, curve *5*). In the sample volume the grain boundaries are surrounded with wide (about $\sim 50\,\mu$m) regions with reduced luminescence

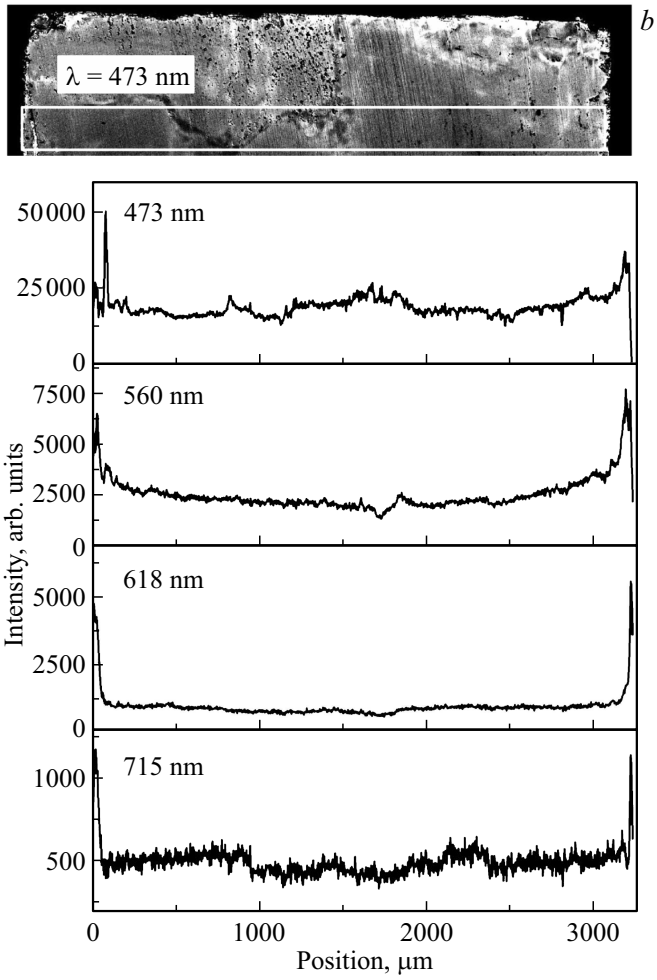

Fig. 4 (*cont.*).

intensity in the whole spectral range (including the red luminescence).

4. Discussion of results

According to experimental data, ZnSe annealing in argon and selenium results in significant spatial inhomogeneity of luminescence characteristics of the samples. In the band *1* the strips, parallel to the sample surface, with a width of hundreds micrometers, with various luminescence intensity in one spectral range or another, are observed. The similar inhomogeneity of luminescence characteristics was observed in ZnSe crystals, doped with Fe and Cr [16,17]. In study [18] it was shown that such inhomogeneity is typical for semiconductors with IDC concentration gradients. Usually these gradients are formed as a result of diffusion of impurities or intrinsic point defects. Most likely, inhomogeneity in ZnSe crystals, annealed in argon or selenium, is also formed due to point defects diffusion. This is confirmed by the fact that strip boundaries are distorted in case of crossing them with grain boundaries. It is known that point defects diffusion along grain boundaries runs faster. In case of ZnSe, annealed in zinc vapors, there was no such inhomogeneity. In these samples the high luminescence intensity is registered in regions, adjacent to the crystal surface, including impurity atmospheres around grain boundaries. This inhomogeneity is not similar to ILIR, but looks like a decoration of large-scale structure defects. Study [19] reported on study of luminescence characteristics of CVD–ZnSe samples, subject to gasostatic processing in argon: $T = 1200^\circ$C, $P = 90$ MPa, for 53 h. Luminescence of these samples was homogeneous on a macroscopic scale. Luminescence spectrum was close to initial polycrystal spectrum with a bit higher IDC luminescence intensity.

These results allow to assume that at ZnSe annealing in argon and selenium, the primary evaporation of zinc from the crystal surface is happened. In study [20] it was shown that at annealing temperature of $> 900^\circ$C zinc atoms prevail in the vapor phase. As a result, bands with increased zinc vacancies concentration, reduced zinc interstitial atoms concentration and selenium excess are formed near the surface. In case of annealing in selenium the value of these effects should be higher than in case of annealing in argon. As a result, the diffusion profiles of intrinsic point defects concentrations will be formed in these crystals due to diffusion from the volume. In case of annealing in zinc vapors the process of zinc evaporation from the surface is complicated, the saturation of near-surface region with interstitial zinc, that decorates the surface defects and grain boundaries, is performed.

Also, during annealing in all atmospheres the coarsening of ZnSe grains and dissolution of increased IDC concentration regions, registered in initial ZnSe, are performed. Also, during annealing the residual impurities and intrinsic point defects can diffuse to drains as grain boundaries and crystal surface, as well as their precipitation. Thus, during annealing of ZnSe samples the several processes happen in them, that significantly impact both the impurity-defect composition of crystals and spatial distribution of IDC in them. All these processes result in the registered experimentally complex situation of spatial distribution of luminescence characteristics in crystals, subject to high temperature annealing. In case of gasostatic processing the processes of intrinsic point defects evaporation and adding into crystal are complicated and intrinsic point defects concentration in near-surface band is relatively stable. Only „internal“ processes — grains coarsening, precipitation, etc., appear in such samples. As was shown in study [19], there are no qualitative changes in impurity-defect composition and spatial distribution of luminescence (except for grains coarsening) as a result of gasostatic processing. Thus we can state that the processes of intrinsic point defects evaporation and adding are responsible for the effects observed in this study.

It seems, that the strips, observed in ZnSe−Ar and ZnSe−Se, with increased and reduced luminescence (ILIR and RLIR) are related to the profiles of intrinsic point defects concentration (vacancies and interstitial atoms of zinc and selenium) formed in them. These intrinsic point defects can form various IDC both between themselves and with residual impurities. Spatial distribution of these IDC will be defined with concentration profiles, that form their intrinsic point defects. Recombination of nonequilibrium carriers through these IDC results in formation of the observed strips. If recombination is radiative in spectral interval, registered in this study, ILIR will be observed. In case of non-radiative recombination or luminescence in ranges outside of $0.5-0.72\,\mu$m, RLIR will be registered. In case of ZnSe−Zn, zinc, added from atmosphere, is probably actively captured by structure defects in near-surface layer and by adjacent grain boundaries. Zn interaction with residual impurities results in formation of large amount of IDC, related to large-scale structure defects. Specifics of this surface resulted in high luminescence intensity of these IDC in the examined spectrum range. The observed information on spatial distribution of luminescence characteristics allows to make some specific assumptions on processes, happened during annealing, and nature of IDC in annealed crystals. In ZnSe−Ar crystal the region *1* is characterized with low luminescence intensity in the range registered in this study. Most likely, the carriers recombination in this band is performed through IDC without radiation or with radiation outside of range of $0.44-0.75\,\mu$m. Considering that this band should have high concentration V_{Zn}, we can assume that they are included in these IDC (IDC−V_{Zn}).

It should be noted that in study [19] the line in a range of 1300−1400 nm, observed in CVD−ZnSe, grown in similar mode, was related to V_{Zn}. It seems that concentration V_{Zn} and, consequently, IDC−V_{Zn} decrease fast with removal from the sample surface and closer to the end of the band *1* their contribution to carriers recombination becomes insignificant. In the same band ILIR with IDC, that luminesce in a range of 560 nm, is formed. Considering that this ZnSe−Ar region has high concentration of excess selenium, it is reasonable to assume that these IDC include Se (IDC−Se). Concentration of excess selenium (and, consequently, IDC−Se) also decreases with removal from the surface. If concentration drop of IDC−Se is slower than IDC−V_{Zn}, the conditions for ILIR arise [18]. With the further increase of the distance from the surface the significance of IDC−Se decreases. The observed increase of luminescence intensity in the same range is probably related to long-wave tail of strip 520−540. With decrease of IDC−V_{Zn} and IDC−Se influence on carriers recombination the possibility of recombination through excitons increases. Therefore, the exciton luminescence intensity increases. It reaches maximum at distance of $\sim 550\,\mu$m from surface. Then it drops and at distance of $750\,\mu$m it reaches the plateau. It can be explained by assumption that during annealing the large amount of IDC is formed in ZnSe−Ar, including V_{Se}. Recombination through these IDC (IDC−V_{Se}) is performed without radiation or with radiation outside of the registered spectral range. It should be noted that in study [21] the lines 830 and 960 nm were related to V_{Se}. Concentration of these IDC drops closer to surface due to annihilation of V_{Se} with excess selenium, coming from the surface layer enriched with it. In the band *1* these IDC influence is small, but with increase of distance from the surface the significance of IDC−V_{Zn} and IDC−Se reduces and at distances of more than $500\,\mu$m the influence of IDC−V_{Se} becomes significant. At distance of $750\,\mu$m from surface the factor of excess selenium flow influence becomes negligible and concentration of IDC−V_{Se} and its influence on exciton luminescence is stabilized. Situation with spatial dependence of luminescence intensity of strip 520−540 nm can be generally explained the same as the dependence of exciton luminescence, if IDC, providing luminescence of this strip, are uniformly distributed over the sample. However, there is one difference in spatial dependencies of luminescence intensity of exciton line and strip 520−540 nm — in the band *1* the luminescence exciton intensity increases, and it is likely that there is no strip 520−540 nm. With the further removal from surface these dependencies are close. This difference can be explained with assumption, that IDC, responsible for strip 520−540 nm, include interstitial zinc (IDC−Zn_i). In this case, since the concentration of interstitial zinc Zn_i in the band *1* is low, luminescence of this band of strip 520−540 nm can be suppressed. With the further removal from surface the concentration of Zn_i and, correspondingly, IDC−Zn_i is stabilized and spatial dependence of luminescence intensity of strip 520−540 nm coincides with the similar dependence of exciton luminescence. The similar processes (considering significantly higher concentration of excess selenium and zinc vacancies) can explain the situation in ZnSe−Se. Recombination through IDC−V_{Se} due to high concentration of these centers almost completely suppresses exciton luminescence and luminescence of strip 500−520 nm in the band *1*. Significantly higher excess of selenium destroys IDC−V_{Se} complexes in the whole crystal volume. As a result, there is no drop of intensity of exciton luminescence and luminescence of strip 500−520 nm with large removal from surface. Since ILIR on wavelength of 560 in ZnSe−Ar is related to excess selenium diffusion from surface and IDC−Se formation, it is natural that ILIR appearance in ZnSe−Se crystal on wavelength of 560 nm is related to the similar reasons. Strip 520−540 nm can transform to strip 500−520 nm due to formation of new IDC and recombination of IDC−Zn_i. These processes can be related with excess selenium in the whole crystal or with various point defects release after IDC−V_{Se} breakdown. It should be noted that in similar crystals of CVD−ZnSe in crystal regions with excess selenium, in study [17], the luminescence spectra close to strip 500−520 nm were observed. In article [22] the line near 500 nm was also related to excess selenium.

Nature of IDC, forming the red lines, is uncertain. In study [23] the lines in this range were associated with luminescence, isolated with V_{Zn}. This is confirmed with the fact that their luminescence is registered in the band *1* of ZnSe−Ar and ZnSe−Se. However, based on this hypothesis, it is hard to explain the increase of luminescence intensity of these lines at removal from crystal surface. Their luminescence intensity is low, that complicates their study; it is possible that this group of lines is formed by IDC of different nature.

In ZnSe−Zn, as in case of gasostatic processing, no significant changes in impurity-defect composition and crystal homogeneity are observed. Luminescence of the main part of this crystal is sufficiently homogeneous and close to luminescence of region *2* of ZnSe−Ar. This allows to assume that nature of IDC, forming the strips 520−540, is the same. The fact that this strip intensity increases in near-surface band, where interstitial zinc concentration should be high, confirms the assumption that IDC−Zn_i actually includes interstitial zinc.

Nature of strip 630, clearly registered in near-surface band of ZnSe−Zn, is uncertain. Considering that its intensity is maximum in the band, where high excess concentration of zinc is assumed, it is reasonable to relate it with this defect. However the similar line is observed on a tail of strip 500−520 in ZnSe−Se. Of course, the abovementioned picture of impurity-defect composition and its distribution in crystals after heat treatments is of preliminary nature only. The abovementioned processes, that can happen during annealing, result in the observed complex picture in spatial distribution of luminescence characteristics in volume of ZnSe crystals, grain boundaries and structure defects. To make sense of it, the additional experiments of isothermal annealing and gasostatic processing at similar temperatures and other methods use (particularly, methods of surface chemical composition analysis) are required.

5. Conclusion

In conclusion let's summarize the main results and findings of the performed study.

1. ZnSe annealing at 1000°C in gaseous atmospheres at low gas pressure results in significant changes of impurity-defect composition and significant inhomogeneity of spatial distribution of luminescence characteristics in a range of $0.45-0.72\,\mu$m of crystals, especially in near-surface band with a width of several hundreds micrometers.

2. ILIR and RLIR are registered in ZnSe−Ar and ZnSe−Se, indicating the diffusion nature of processes during annealing in these crystals.

3. Based on spatial distribution of luminescence characteristics the assumptions are made on composition of IDC formed during annealing.

Funding

The study was performed using equipment of the Research Equipment Sharing Center of the „Analytical center of the Federal Government Budgetary Institution of the Federal Research Center of the Institute of General Physics of the Russian Academy of Sciences“ with partial financial support through the grant of the Russian Foundation for Basic Research No. 18-29-20048, in part related to development of technology and production of samples; the study was supported with grant of the Russian Scientific Foundation No. 19-13-00205.

Conflict of interest

The authors declare that they have no conflict of interest.

References

[1] S.B. Mirov, V.V. Fedorov, D. Martyshkin, I.S. Moskalev, M. Mirov, S. Vasilyev. IEEE J. Select. Top. Quant. Electron., **21** (1), (2015)
[2] S. Vasilyev, I. Moskalev, M. Mirov, V. Smolski, D. Martyshkin, V. Fedorov, S. Mirov, V. Gapontsev. Proc. of SPIE, Ultrafast Bandgap Photonics II (Anaheim, California, US, 2017) v. 10193.
[3] S.V. Kurashkin, O.V. Martynova, D.V. Savin, E.M. Gavrishchuk, S.S. Balabanov, V.B. Ikonnikov, V.V. Sharkov. Phys. Lett., **16**, 075801 (2019).
[4] A.A. Gladilin, E.S. Gulyamova, V.P. Danilov, N.N. Il'ichev, V.P. Kalinushkin, I.N. Odin, P.P. Pashinin, R.R. Rezvanov, A.V. Sidorin, M.I. Studenikin, V.A. Chapnin, M.V. Chukichev. Quant. Electron., **46** (6), 545 (2016).
[5] N.N. Il'ichev, A.A. Gladilin, E.S. Gulyamova, V.P. Kalinushkin, S.A. Mironov, A.V. Sidorin, P.P. Pashinin, V.V. Tumorin, E.M. Gavrishchuk, D.V. Savin, S.A. Rodin, V.B. Ikonnikov, M.V. Chukichev. Quant. Electron., **50**, (8) 730, (2020).
[6] O. Gafarov, A. Martinez, V. Fedorov, S. Mirov. Optical Mater. Express, **7** (1), 25 (2017).
[7] S.A. Rodin, E.M. Gavrishchuk, V.B. Ikonnikov, D.V. Savin. Inorg. Mater., **54** (1), 21 (2018).
[8] N.A. Timofeeva, E.M. Gavrishchuk, D.V. Savin, S.A. Rodin, S.V. Kurashkin, V.B. Ikonnikov, T.S. Tomilova. Inorg. Mater., **55**, 1274 (2019).
[9] D.D. Nedeoglo, A.V. Simashkevich. *Electric and Luminescent Properties of Zinc Selenide* (Kishinev, Shtiintsa, 1984).
[10] Yu.F. Vaksman Yu.A. Nitsuk, V.V. Yatsun, A.S. Nasibov, P.V. Shapkin. Semiconductors, **45**, 1129, (2011).
[11] G. Colibaba, M. Caraman, I. Evtodiev, S. Evtodiev, E. Goncearenco, D. Nedeoglo, N. Nedeoglo. J. Luminesc., **145**, 237 (2014).
[12] I. Abbasov, M. Musayev, J. Huseynov, M. Kostyrko, S. Babayev, G. Eyyubov, S. Aliyeva. Ukr. J. Phys. Opt., **21** (2), 103 (2020).
[13] V.P. Kalinushkin, O.V. Uvarov. ZhTF, **86** (12), 119 (2016) (in Russian).
[14] V.P. Kalinushkin, O.V. Uvarov, A.A. Gladilin, J. Electron. Mater., **47**, 5087 (2018).

[15] N.K. Morozova, E.M. Gavrishchuk, I.A. Karetnikov, O.R. Golovanova, V.S. Zimogorskii, V.G. Galstyan. ZhPS, **63** (5), 731 (1996) (in Russian).
[16] A. Gladilin, O. Uvarov, S. Mironov, N. Timofeeva, E. Gavrischuk, V. Kalinushkin. Acta Phys. Polon. A, **136** (4), 637, (2019).
[17] S. Balabanov, E.M. Gavrishchuk, A.A. Gladilin,V.B. Ikonnikov, N.N. Il'ichev, V.P. Kalinushkin, S.A. Mironov, D.V. Savin, M.I. Studenikin, N.A. Timofeeva, O.V. Uvarov, V.A. Chapnin. Inorg. Mater., **55** (5), 423, (2019).
[18] V.P. Kalinushkin, O.V. Uvarov, S.A. Mironov, K. Nartov, N.N. Il'ichev, M.I. Studenikin, E.M. Gavrischuk, N.A. Timofeeva, S.A. Rodin, A.A. Gladilin. J. Luminesc., **231**, 117795 (2021).
[19] E.M. Gavrishchuk, A.A. Gladilin, V.P. Danilov, V.B. Ikonnikov, N.N. Il'ichev, V.P. Kalinushkin, A.V. Ryabova, M.I. Studenikin, N.A. Timofeeva, O.V. Uvarov, V.A. Chapnin. Neorg. mater., **52** (11), 1180 (2016) (in Russian).
[20] S.A. Medvedev, V.N. Martynov, S.P. Kobeleva, N.D. Ahmed-Zade. Elektr. tekhn., ser. Materialy, vyp. 11, 87 (1980) (in Russian).
[21] N.K. Morozova, I.A. Karetnikov, V.V. Blinov, E.M. Gavrishchuk. FTP, **35** (5), 534 (2001) (in Russian).
[22] S. Kishida, K. Matsuura, H. Mori, T. Yanagawa, I. Tsurumi, C. Hamaguchi. Phys. Status Solidi A, **106**, 283 (1988).
[23] K.M. Lee, Le Si Dang, G.D. Watkins. Sol. St. Commun., **35** (7), 527, (1980).